Modelling based radiography for NDE of subsea pipelines

Misty I. Haith, Uwe Ewert, Stefan Hohendorf, Carsten Bellon, Andreas Deresch, Peter Huthwaite, Michael J. S. Lowe, and Uwe Zscherpel

Citation: AIP Conference Proceedings **1706**, 110004 (2016); doi: 10.1063/1.4940575
View online: http://dx.doi.org/10.1063/1.4940575
View Table of Contents: http://scitation.aip.org/content/aip/proceeding/aipcp/1706?ver=pdfcov
Published by the AIP Publishing

Modelling Based Radiography for NDE of Subsea Pipelines

Misty I. Haith[1,a)], Uwe Ewert[2], Stefan Hohendorf[2], Carsten Bellon[2], Andreas Deresch[2], Peter Huthwaite[1], Michael J.S. Lowe[1] and Uwe Zscherpel[2]

[1]*Imperial College, Department of Mechanical Engineering, London, United Kingdom*
[2]*BAM Federal Institute for Materials Research and Testing, Berlin, Germany*

[a)]Corresponding author: misty.haith09@imperial.ac.uk

Abstract. This work presents the use of limited experimental measurements to develop a set of calibrated simulation parameters that can then be used for reliable simulation of subsea pipeline inspections. The modelling software aRTist is used as the simulation tool, and the calibration is through comparison with experimental images of a well characterised sample in a water tank. Image quality parameters such as signal-to-noise ratio, contrast and basic spatial resolution are compared with the aim of matching simulated values to experimental results. Currently the model is partially calibrated, with signal-to-noise ratio successfully matched while differences are still found in contrast-to-noise ratio comparisons. This means that measurements depending on absolute intensity are not accurate enough in the simulation at this stage. However, the simulation is found to be accurate for wall thickness measurements in tangential images, which are not based on absolute intensity, with simulated and experimental cases producing similar results.

INTRODUCTION

Accurate and reliable detection of subsea pipeline corrosion is required in order to verify the integrity of the pipeline. Often a pipeline can be inspected internally by pigging, however where this cannot be applied external examination must be used. Radiography holds a significant advantage over many other NDT methods in that it does not require surface preparation or insulation removal; in addition it is less sensitive to naturally grown external deposits on the pipe surface than other inspection techniques. Subsea radiography often exploits modern digital detectors, and thus has great potential to benefit from the advantages these offer. Identifying the most suitable imaging setups is crucial, both for cost effectiveness and reliable detection and sizing of defects. Figure 1 shows established radiographic methods for pipeline corrosion imaging, as described in the standards (EN 16407 [1, 2]).

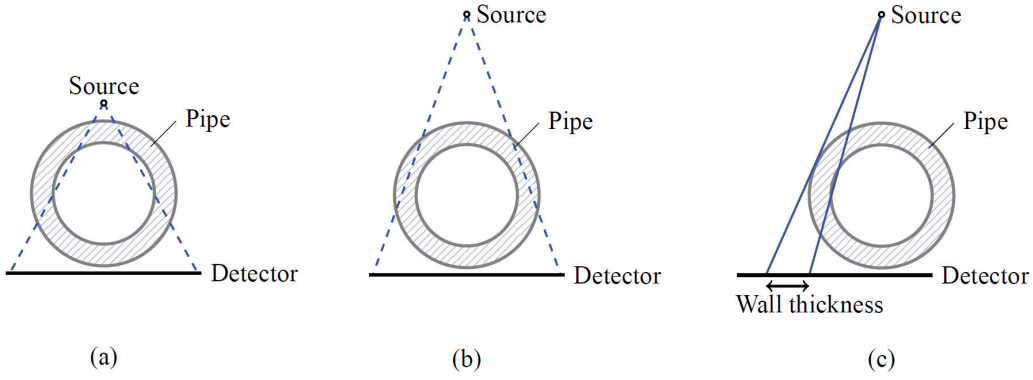

FIGURE 1. Different methods of radiographic imaging of pipelines for corrosion. (a): Double Wall Single Image (EN 16407: part 2 [2]), (b): Double Wall Double Image (EN 16407: part 2), (c): Tangential (EN 16407: part 1 [1])

42nd Annual Review of Progress in Quantitative Nondestructive Evaluation
AIP Conf. Proc. 1706, 110004-1–110004-8; doi: 10.1063/1.4940575

The method currently used for experimental subsea imaging is Double Wall Single Image (DWSI), shown in Fig 1(a). In this method the source and detector are placed close to each side of the pipe. As the upper wall is very close to the source any features are magnified across the whole detector, meaning that this method effectively just images the lower pipe wall, close to the detector. Corrosion is visible from the intensity change it causes, as more radiation reaches the detector in areas where the wall is thinner. The DWSI method is used in the current hardware as the relatively short source-to-detector distance reduces the highly attenuating and scattering effects of the water. A variant of double wall imaging is Double Wall Double Image (DWDI), shown in Fig 1(b), in which the source is set back from the pipe. In this case the upper wall is not magnified to the same extent, and both upper and lower pipe walls can be clearly imaged in a single exposure. In tangential imaging, Fig 1(c), the source is set back as in DWDI but the detector is offset such that the edge of the pipe is visible in the radiograph. Wall thickness at the tangential position can be measured on the resulting radiograph directly, as the inner and outer wall positions are points of major intensity change and therefore identifiable in a profile across the image.

Standards for radiographic imaging of pipeline corrosion do not currently cover underwater conditions, and as water is highly scattering it can have a significant impact on radiographic image quality: thus it is vital to investigate inspection configurations with water. Subsea radiography is extremely costly, and extensive experimental data for research is difficult to obtain. Simulations are significantly more affordable and accessible than subsea experimental data, and are able to model a wide range of underwater radiographic setups. However, simulation models have not been validated as accurate for underwater imaging, and before conclusions can be drawn from simulation results they must be shown to be comparable to experimental results. In this work we aim to validate the simulation tool aRTist[1] for use simulating underwater radiography in these configurations. To do this we obtain a set of experimental radiographs of a well characterised pipe in water and simulate the same setups in aRTist. The experimental data is used to adjust aRTist parameters with the aim of matching simulated radiographs to experimental ones. Experimental and simulation methods are described in the next section, followed by methods of tuning the simulation and matching image quality.

METHOD

Experimental Method

Experiments were performed in the high-energy X-ray laboratory at BAM, Berlin, Germany. The pipe used for testing and the experimental setup are shown in Figure 2. The sample, Fig 2(a), was a stepped pipe with an outer diameter of 322.6 mm and wall thickness from 8.5 mm to 25 mm. The pipe also has three sets of internal flat bottomed holes with depths of 10%, 20% and 50% wall thickness. The experimental setup, Fig 2(b), used a pulsed betatron with a maximum energy of 7.5 MeV [3] and a flat panel detector. The detector (Perkin Elmer XRD 1621 model [4]) has a sensitive area of 409.6 mm x 409.6 mm with 2048 x 2048 pixels and a pixel size of 200 μm. To provide higher grey values the detector was used in pixel binning mode, with 1024 x 1024 pixels of 400 μm.

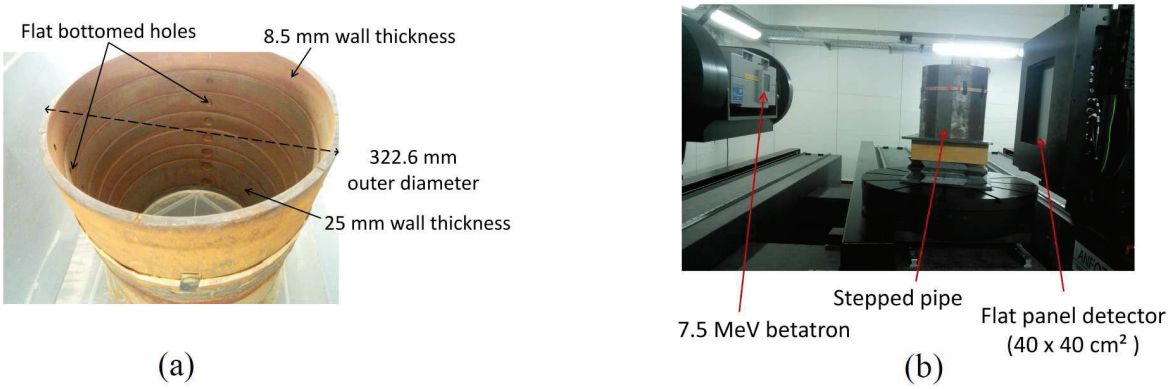

FIGURE 2. (a) Stepped pipe used as test object, (b) Setup for high energy radiography of the pipe

[1] analytical RT inspection simulation tool - licensed by BAM (www.artist.bam.de)

A source to detector distance of 1650 mm was used, with a pipe centre to detector distance of 504 mm. Due to equipment constraints it was not possible to move the source or detector closer to the pipe, as required for the double wall single image method. Instead images were taken with the double wall double image or tangential methods. All images were taken with the same exposure time of 2 s per frame and the same calibration, using a 100 frame gain image and a 20 frame offset image. Copper filters (1 mm thickness) were used at the source and/or detector in some images to improve image quality.

In order to add water to the setup the pipe was placed in the centre of a rectangular plastic water tank. This allowed for setups with two different water thicknesses to be imaged by rotating the water tank, as illustrated in Figure 3. Silicone was used to create a seal around the base of the pipe allowing for images to be taken with water around the pipe but air inside, in addition to those with water both inside and outside the pipe.

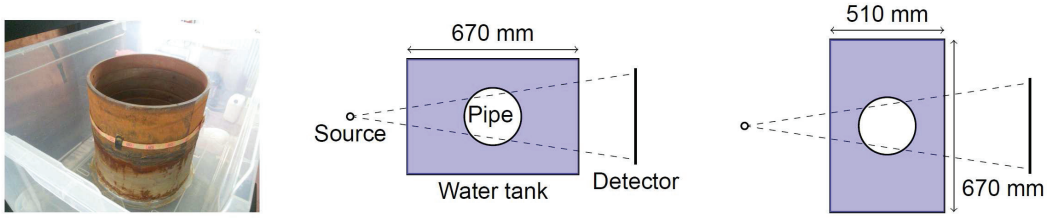

FIGURE 3. (a) The stepped pipe was placed in a rectangular water tank, (b) & (c) show two setups with different water thicknesses made possible by rotating the water tank.

Simulation Method

The same setups as used experimentally were simulated in aRTist, a simulation tool developed by BAM. A visualisation of the simulation setup is shown in Figure 4.

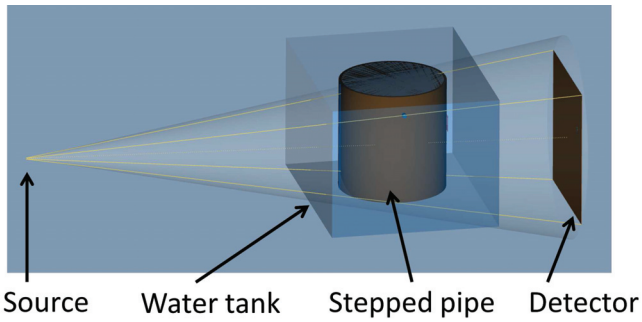

FIGURE 4. Radiographic setup modelled in aRTist. Dimensions and distances used were as in experimental setups.

Further details on aRTist can be found in [5] and [6]. The betatron source was modelled with the spectrum calculator incorporated into aRTist [7], while the detector was modelled using a new Detector Calculator module [8] which uses data from an experimental reference image to characterise the detector.

Image Quality Parameters & Simulation Tuning

The simulation was adjusted with the aim of matching the main image quality parameters to those measured experimentally. These include Signal-to-Noise ratio (SNR), Contrast-to-Noise ratio (CNR) and basic spatial resolution ($SR_b^{detector}$).

Signal-to-noise ratio is defined as the ratio of the mean value of the grey value to the standard deviation of the grey value in a given region of the image [1]. In practice a rectangular region of interest is taken in an area of the image free from significant intensity changes. For each horizontal line of pixels i, with n pixels per line, the mean grey value ($\overline{GV_i}$) and standard deviation (σ_i) are given by [9]:

$$\overline{GV_i} = \frac{1}{n}\sum_{j=1}^{n} GV_{ij} \tag{1}$$

$$\sigma_i = \sqrt{\frac{1}{n-1}\sum_{j=1}^{n}(GV_{ij} - \overline{GV_i})^2} \tag{2}$$

where GV_{ij} is the grey value at line i and column j in the region of interest. These are calculated for each horizontal line of pixels, where there are N lines. Signal-to-noise ratio is then given by:

$$SNR = \frac{Median\left[\overline{GV_i}\right]_{i=1}^{N}}{Median[\sigma_i]_{i=1}^{N}} \tag{3}$$

This is the unnormalised SNR, however as the same equipment and calibration was used for all images the unnormalised value is a suitable measure to evaluate. SNR was measured in experimental images and could be varied in simulated images by changing the number of frames per image in the simulation.

The contrast, C, of an object in a radiograph is given by [10]:

$$C = I - I_{obj} = \Delta I \tag{4}$$

where I_{obj} is the intensity measured on the object indication and I the intensity nearby. The contrast-to-noise ratio can then be calculated from:

$$CNR = \frac{|\Delta I|}{\sigma} \tag{5}$$

where σ is the standard deviation measured in an area near the intensity measurements. CNR is more difficult than SNR to vary independently in the simulation, so measurements from simulated and experimental images were compared and analysed.

Basic spatial resolution is measured with a duplex wire IQI placed on the detector in the experimental radiographs. Basic spatial resolution is determined from the smallest number of the duplex wire pair which is separable by a profile function with less than 20% modulation depth in a linearized profile [11]. $SR_b^{detector}$ measured from experimental images is an input parameter to the detector calculator module in aRTist, ensuring a match of simulation to experiment in this case.

In addition to matching the main image quality parameters, the profile across the edge of the pipe in tangential images was also taken and compared in simulated and experimental cases. Taking a line profile across the radiograph, the edge profile is a portion of this in which the edge of the pipe is visible, as visualised in Figure 5(a). Figure 5(b) shows the grey value (intensity) versus pixel plot for this portion of the radiograph, where the pixel refers to the detector pixel number and is equivalent to a distance along the radiograph. In aRTist the 'long range unsharpness' and 'unsharpness ratio' are two parameters which affect the shape of the profile. Results of simulations with example values of low, medium and high unsharpness are plotted to illustrate the effects of these parameters, along with the experimental profile. The unsharpness parameters were varied to get a similarly shaped profile to experimental results.

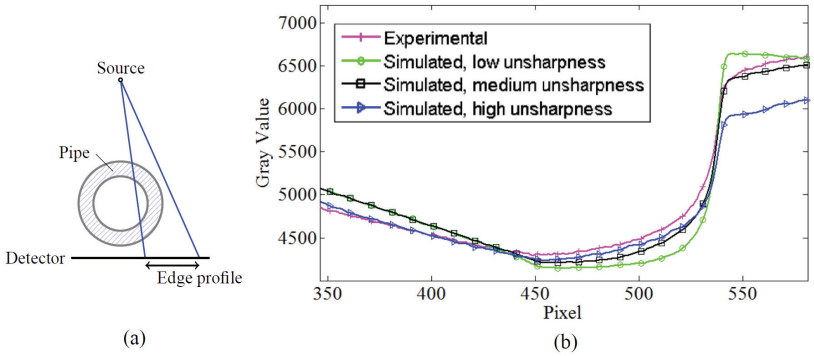

FIGURE 5. (a) Diagram illustrating the edge profile, a portion of the line profile across the radiograph in which the edge of the pipe is visible, (b) The edge profiles of experimental and simulated images are plotted. The minimum intensity seen at pixel 451 identifies the inner pipe wall position, while the outer pipe wall is at the point at pixel 542 where the rate of increase in intensity suddenly stops or slows significantly.

RESULTS

An example of an experimental tangential radiograph with points of interest highlighted is shown in Figure 6.

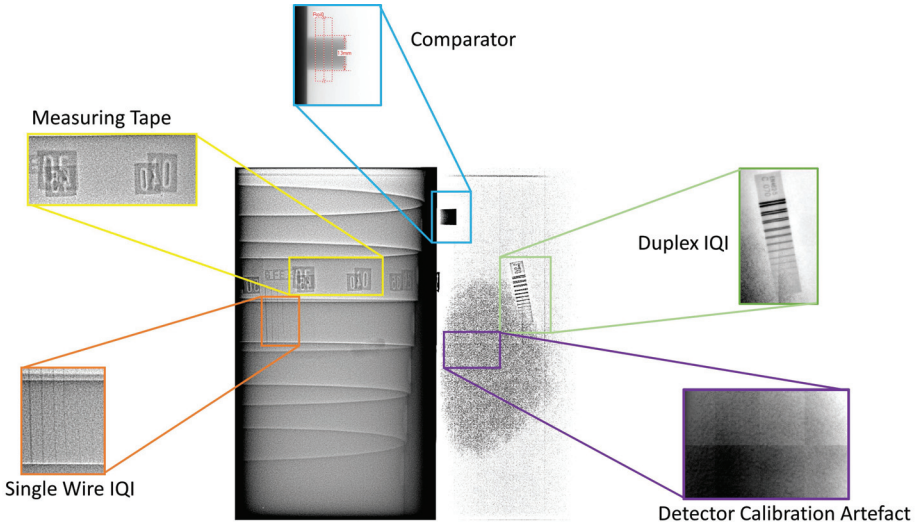

FIGURE 6. An example of an experimental tangential radiograph. It has been high pass filtered for better visualisation and points of interest are highlighted. A 13 mm comparator was fixed to the edge of the pipe to calibrate dimensions in the image. A measuring tape with lead numbers was wrapped around the pipe. A single wire IQI was placed on the outer pipe wall, on the side nearest the detector while a duplex wire IQI was placed on the detector in the free beam area of the image. Although a detector calibration was applied there are still some step-like artefacts visible in the free beam area of some of the images.

Profiles across simulated and experimental images were taken and compared. Similar to the edge profile, these profiles include the edge of the pipe and a distance to either side. Figure 7 shows simulated and experimental profiles for (a) the setup with no water either inside or outside the pipe, and (b) the setup with water outside the pipe but not inside.

Examining these profiles it can be seen that there is an offset in intensity in some areas. The differences in simulated and experimental intensity values means that the intensity based measurements of double wall imaging in

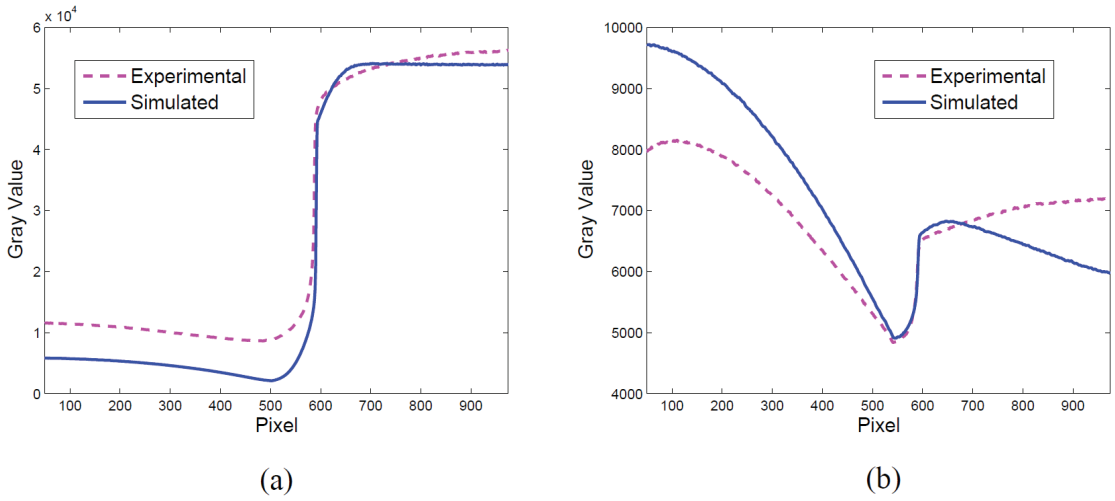

FIGURE 7. Profiles across the radiograph for experimental and simulated images in the cases of (a) No water, (b) With water outside the pipe but not inside. In (a) pipe wall inner and outer positions are visible at pixels 510 and 605 while in (b) they are at pixels 550 and 600.

simulated images will not match the same measurement in experimental images. The cause of this offset is unclear but should be addressed by future work. However, tangential imaging does not depend on the particular intensity values but on the positions of the inner and outer pipe wall given by the minimum intensity (inner wall) and the point where the sharply increasing intensity stops or slows significantly (outer wall). From the profiles in Fig 7 it can be seen that these pipe wall positions are fairly accurately reproduced in the simulated results, meaning tangential measurements may be equivalent to experimental results.

To test this, wall thickness measurements were taken of the thickest, 25 mm, pipe wall in a set of images. Results are shown in Figure 8 for one simulated and experimental image in each of the five setups used: those with water both inside and outside the pipe and with either the longer, 670 mm, or shorter, 510 mm, water tank thickness, those with water just outside the pipe and with the 670 mm or 510 mm thickness and finally those with no water. All measurements are within ±0.8 mm of the actual value, and although the simulated results tend to be lower than experimental ones this difference is fairly small. Analysis of more images is needed but an initial conclusion is that the simulation produces results comparable to experimental ones for tangential measurements.

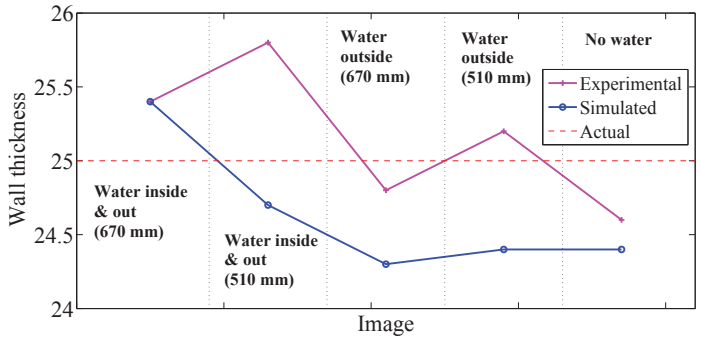

FIGURE 8. Wall thickness measurements of the 25 mm pipe wall in tangential experimental and simulated images for the five different setups used.

Contrast-to-noise and signal-to-noise ratios were also measured and compared in experimental and simulated

images. CNR was measured across several pipe wall steps in each radiograph and results averaged to get a single value to compare for each image. Figure 9 shows the CNR for images in all five setup types. Images are numbered with 1 – 5 referring to the setup type, while a – d refers to the copper filter used, as labelled in the figure.

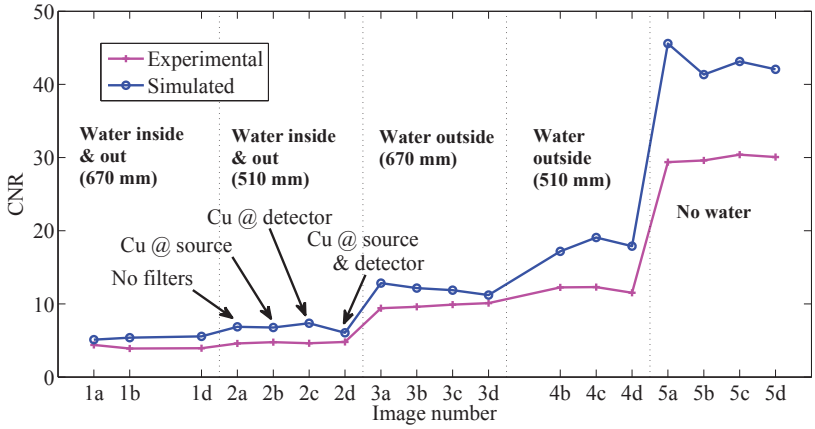

FIGURE 9. Contrast-to-noise ratio for a series of simulated and experimental images in the five different setup types. The images were all taken with 100 frames. Copper filters were used in some images, labelled a – d where a = no filter, b = 1 mm copper at the source, c = 1 mm copper at detector and d = 2 mm copper in total with 1 mm at both source and detector.

From Fig 9 it can be seen that the simulated CNR values are higher than the experimental ones. This is the same problem as seen in the profile comparisons, and once that issue has been identified and accounted for it is expected that the simulated CNR will also match that from the experiment. However, although the CNR values differ, the same overall trend of increasing CNR with decreasing water thickness seen experimentally is reproduced in the simulation results. This demonstrates that the model takes into account the effects of water and accurately responds to changes in water thickness.

SNR was also measured, near to the CNR measurement points, and similarly averaged. Results are shown in Figure 10. In the case of SNR both the absolute values and overall increasing trend of experimental measurements are reproduced in the simulated results. This is an encouraging result as the frame number used in the simulations, which directly affects SNR, was tuned using experimental images from only one setup type. All simulated images were then taken with the same frame number, with the agreement in trend again demonstrating that the effects of water are being taken into account correctly by the model.

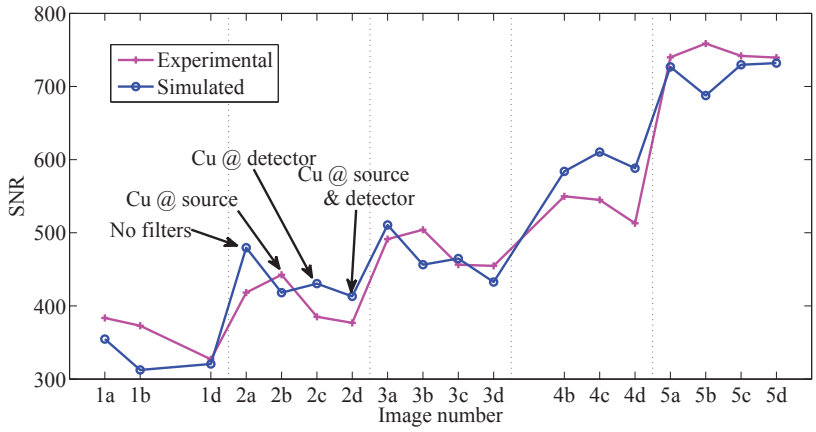

FIGURE 10. Signal to noise ratio for the same set of images as in Fig 9.

SUMMARY

The aim of this work is to calibrate a radiographic simulation model for use accurately simulating underwater radiography. The model can then be used to simulate a wide range of subsea pipeline inspection scenarios. A set of experimental data has been obtained and used to adjust simulation parameters, aiming to match simulated results to the experimental ones. Currently the model is partially calibrated, producing matching signal-to-noise ratios and the correct trend in contrast-to-noise. However the profile across the radiograph and the absolute CNR do not match sufficiently. Work investigating these remaining differences is ongoing. Once calibrated the simulation will be used to help identify optimum subsea pipeline imaging setups.

ACKNOWLEDGEMENTS

This work was supported by EPSRC grant EP/I017704/1, with a contribution from BP. The Royal Commission for the Exhibition of 1851 also provided a financial contribution towards this work.

REFERENCES

1 EN 16407-1: 2014, Non-destructive testing - Radiographic inspection of corrosion and deposits in pipes by X- and gamma rays - Part 1: Tangential radiographic inspection.

2 EN 16407-2: 2014, Non-destructive testing - Radiographic inspection of corrosion and deposits in pipes by X- and gamma rays - Part 2: Double wall radiographic inspection.

3 JME Portable 7.5 MeV X-ray Betatron for Radiographic Non-Destructive Testing, User Manual, Issue 1, 2006.

4 XRD 1621 Detector Series, Basic Specifications and Potential Applications of Digital Flat Panel Detectors, www.perkinelmer.com.

5 C. Bellon, A. Deresch, C. Gollwitzer, and G.-R. Jaenisch, "Radiographic Simulator aRTist: Version 2," in *Proc. of 18th World Conference on Nondestructive Testing* (Durban, South Africa, 2012) www.ndt.net/article/wcndt2012/papers/333_wcndtfinal00333.pdf.

6 G.-R. Jaenisch, A. Deresch, C. Bellon, U. Ewert, and W. Przybilla, "Measurement and modeling of scatter ratios at high energies," in *review of Progress in Quantitative Nondestructive Evaluation*, eds. D. O. Thompson and D. E. Chimenti (American Institute of Physics 1335, Melville, NY) **30**, 517-524 (2011).

7 A. Deresch, G.-R. Jaenisch, C. Bellon, and A. Warrikhoff, "Simulation and Experimental Verification of X-Ray Spectra," in *review of Progress in Quantitative Nondestructive Evaluation*, eds. D. O. Thompson and D. E. Chimenti (American Institute of Physics 1211, Melville, NY) **29**, 535-540 (2010).

8 A. Deresch, M. Jechow, and C. Gollwitzer, "Spectral characterization of storage phosphor imaging plates," in *review of Progress in Quantitative Nondestructive Evaluation*, eds. D. O. Thompson and D. E. Chimenti (American Institute of Physics 1581, Melville, NY) **33**, 1786-1792 (2014).

9 ASTM E2446 - 05 (Reapproved 2010, Revised 2015 - to be published), Standard Practice for Manufacturing Characterization of Computed Radiography Systems.

10 U. Ewert, U. Zscherpel, and K. Bavendiek, "Strategies for film replacement in radiography - a comparative study," in *PANNDT* (Buenos Aires, Argentina, Oct 22-26 2007).

11 ASTM E2002 - 15 (Reapproved 2009, Revised 2015 - to be published), Standard Practice for Determining Total Image Unsharpness and Basic Spatial Resolution in Radiography and Radioscopy.